Characterisation of precipitation and carbide coarsening in low carbon low alloy Q&T steels during the early stages of tempering

Yulin Ju [a], Aimee Goodall [a], Martin Strangwood [a,b], Claire Davis [b]

[a] School of Metallurgy and Materials, University of Birmingham, Birmingham, UK.
[b] Warwick Manufacturing Group, University of Warwick, Coventry, UK.

Key word: Q&T steels, lath martensite, cementite coarsening, secondary alloy carbides, hardness evolution

Abstract: In order to ensure that appropriate tempering conditions are used to obtain desired strength and toughness for low carbon low alloy quench and tempered (Q&T) steel plates in a range of thickness, it is desirable to be able to predict the effect of composition and tempering conditions (time and temperature) on the microstructure and hence the hardness evolution for these steels. In this paper, carbide precipitation and coarsening behaviour in three low carbon low alloy Q&T steels have been investigated during tempering at 600 °C up to 16 hours to determine the role of alloying additions of Mo, V, Cr and Si. It has been found that auto-tempering occurs during water quenching with ε'-carbide and cementite being present within the martensite laths for all three steels. In the Base steel, cementite becomes the stable second phase after 2 hours tempering and has an elliptical (sometimes spherical) shape, which coarsens with time during tempering from 2 hrs to 16 hrs. However, in the Base-Mo-V and Base-Cr-Mo-V-Si steels, elliptical and needle-shaped cementite (shown to contain Mn, Mo and Cr) both exist during tempering; furthermore, finer elliptical secondary Mo-V-rich carbides are observed after tempering for 4 hrs. The coarsening of cementite contributing to the softening process in the three steels has been quantified with, most significantly, the inter- and intra-lath carbides coarsening independently. Although fine secondary alloy carbides are observed after 4 hours tempering, they do not result in any noticeable secondary hardening peak in the Base-Mo-V and Base-Cr-Mo-V-Si steels.

Introduction

Quenched and tempered (Q&T) steels, which normally have a relatively low carbon content and also contain alloying elements such as Mn, Mo and Cr, are widely used in applications such as cranes and earth movers, due to their desirable mechanical properties combining high

strength and good toughness. Lath martensite normally forms during quenching with the occurrence of auto-tempering due to the low carbon and alloying contents resulting in high Ms temperatures [1-4]. Cementite is observed as the predominant as-quenched carbide in low carbon alloyed steels with relatively high Ms temperatures (>400 °C) [2, 4], e.g. observed in agitated water quenched Fe-0.16C-1.49Mn-0.27Si-0.28Cr-0.048Nb-0.0044V-0.0046Al steel [4]. Whereas, close-packed hexagonal ε-carbides, proposed by Jack using powder diffraction patterns [5], or ε'-carbides with orthorhombic symmetry, named by Taylor [6] with the carbide being partially ordered, have been identified within the laths during quenching for steels with relatively lower Ms temperatures [1, 3], such as after oil quenching of AISI 4340 steel where Ms is approximately 304 °C [3].

Carbide evolution for low carbon low alloy Q&T steels during tempering can be identified as having the following stages: Firstly, transition iron carbides (either ε-carbides or ε'-carbides) form, where the initial temperature for their formation can be observed at temperatures as low as 80 °C [7, 8]. Secondly, with an increase of tempering temperature (over a wide range of temperatures from 200 °C to 350 °C [9]) and time, the transformation from ε/ε'-carbides to cementite occurs, where cementite initially has a high aspect ratio (8 - 10) [9-11]. In the tempering temperature range 400 - 700 °C, cementite particles undergo a spheroidisation and coarsening process [10, 12], where the lath structure can still be observed during the early stage of tempering [13, 14], resulting in a continuous decrease of hardness during tempering [15]. The rate of coarsening for cementite is influenced by the alloying elements present. The carbide-forming substitutional elements, e.g. Mn, Mo, V and Cr, can partition into cementite at higher temperatures resulting in a retardation of coarsening [3, 16, 17]. Si, a non-carbide-forming element, can delay the transformation from ε/ε'-carbides to cementite, stabilise cementite with a fine plate-like structure to high temperatures [10] and delay cementite coarsening [16] with the formation of a Si-enriched layer at the cementite/ferrite interface, reducing the flux of carbon available for cementite coarsening [9, 16, 18]. Cementite tends to be located on the martensite lath boundaries with a relatively larger volume fraction than in the laths [12, 19, 20], and coarsening of inter-lath cementite is quicker than that for intra-lath cementite due to faster solute boundary diffusion [20-22]. Finally, with strong carbide-forming alloying elements (e.g. Mo, Cr, V) added in steels, stable alloy carbides with substantially higher enthalpies of formation are promoted, which retain a smaller size than cementite even during prolonged tempering. Most work on alloy carbides has been carried out on highly alloyed steels, e.g. 2.25 Cr-1 Mo and 9 Cr-1 Mo grades [23-25]. In these, M_2C

carbides are the next type of carbides to form after cementite precipitation in Cr-Mo steels or Cr-Mo-V steels with a high bulk Mo/V ratio during the early stage of tempering [23, 24], which, depending on composition, can be followed by M_7C_3, $M_{23}C_6$ and M_6C to give secondary hardening. M_2C carbides have been reported after tempering for 1 hr at 600 °C and persist after tempering for 100 hrs at 600 °C in a Fe-0.6Cr-0.5Mo steel [23]. However, the effect of lower alloying element levels in Q&T steels still requires elucidation.

The purpose of this investigation is to study the carbide precipitation and coarsening behaviours in three low carbon low alloy S690 steels with different additions of Mo, V, Cr and Si to understand the hardness changes during the early stage of tempering (up to 16 hrs) at 600 °C.

Materials and methods

Three laboratory produced Q&T steel plates were supplied by Tata Steel (UK) that were hot rolled to ~35 mm thickness and air cooled, with the chemical compositions given in Table 1. Samples measuring 15 × 20 × 20 mm (15mm through thickness) were re-austenitised at 925 °C for 1 hour and then quenched into room temperature water, to produce a lath martensitic microstructure. Quenched samples were tempered for 2 hrs, 4 hrs, 8 hrs and 16 hrs at 600 °C to investigate the carbide evolution and coarsening behaviours for the three steels.

The microstructures and particle compositions were examined by scanning electron microscopy (SEM) in a Jeol 7000 system, transmission electron microscopy (TEM) using a Jeol 2100 system and scanning transmission electron microscopy (STEM) using FEI Tecnai F20 and FEI Talos F220X systems. Bright field (BF) images were used to observe the morphology of the carbides; dark field (DF) images and selected area diffraction (SAD) patterns were used to confirm the carbide type. Convergent beam electron diffraction (CBED) patterns were used to calculate the thickness of thin foil specimens to determine the number density for very fine particles which are not resolvable in SEM images. High angle annular dark field STEM (HAADF-STEM) imaging with energy dispersive X-ray spectroscopy (EDS) was utilised to ascertain the carbide compositions. SEM samples were polished to an PO-S finish and lightly etched in 2% nital. Thin foil specimens used for TEM observation were cut from the mid-thickness position of the as-quenched and selected tempered samples, then ground with silicon carbide papers (grit no. 400-800-1200) to approximately 70-80 μm thickness, followed by twin jet electro-polishing with a 5 vol. %

perchloric acid and 95 vol. % acetic acid solution at room temperature using 50 - 60 V potential giving a 0.16 - 0.18 A polishing current. Carbon replica specimens used for the carbide composition measurements were prepared from the etched SEM samples. A carbon film around 20 - 30 nm (colour grey-brown) was deposited on the etched sample surface, which was then scored into squares (around 2 × 2 mm^2) with a sharp razor blade. The squares of carbon film were removed from the sample surface by electrochemical etching using a solution of 5 % HCl in methanol at 3 volts potential, and were then washed in methanol followed by distilled water. Finally, the carbon film squares were removed from the distilled water and mounted on copper grids for TEM examination. Axiovision 4.6.3 image analysis software was used to obtain the particle size (length, width or radius), distributions, number densities and volume fractions and particle separations from SEM or TEM images (approximately 1000 particles measured for each condition assessed).

XRD measurements were carried out using a PANanlytical Empyrean XRD instrument with a cobalt target (wavelength λ=1.78901Å) to determine the lattice parameters for the three steels in the as-quenched condition and after tempering in order to estimate the amount of carbon retained in solid solution. XRD data were recorded in the 2θ range from 45° to 128° with a scanning time of 0.5 hour.

Vickers macro hardness (load 20 kg) testing was used to measure sample hardness, where 25 indents were taken for each sample. Indents were taken 3 mm away from the sample edge to avoid any decarburisation from the heat treatments.

Table 1. The chemical composition and predicted Ms temperature (using the Steven and Haynes equation [26]) for the low carbon low alloy Q&T steels [wt%]

Name	C	Si	Mn	P	S	Cr	Mo	Al	N	Nb	Ti	V	B	Predicted Ms temperature/°C
Base	0.17	0.29	1.2	0.015	0.002	-	-	0.03	0.004	0.03	0.024	-	0.0025	426
Base-Mo-V	0.17	0.28	1.2	0.015	0.002	-	0.5	0.03	0.004	0.03	0.026	0.05	0.0025	423
Base-Cr-Mo-V-Si	0.17	1.24	1.2	0.016	0.002	0.8	0.5	0.04	0.006	0.03	0.027	0.05	0.0025	405

Results

(1) The occurrence of auto-tempering during quenching

All three steels showed an as-quenched lath martensite structure, Figure 1; they also all contained elongated, auto-tempered carbides (detailed coverage below), Figure 2, consistent with the high Ms temperatures (> 400 °C, Table 1). Determination of the zone axis and indices of the in-plane normal to the long axis of the plate / needle-shaped precipitates in the as-quenched condition has been used to construct the great circles of potential habit planes to confirm the type of as-quenched carbides present. These great circles form two groups; the first has a common intersection around the {012}α pole, which would be consistent with ε'-carbides [6], whilst the second group intersects around the {011}α pole - a common habit plane for cementite [27-29], Figure 3, indicating the formation of cementite and ε'-carbides within the martensite laths during quenching in the three steels. As cementite and ε/ε'-carbide align along <110>α and <100>α respectively when the electron beam coincides with the <001>α direction [28, 30, 31], the relative amounts of cementite and ε'-carbide can be determined, Figure 4. In the Base and Base-Mo-V steels, cementite particles are the predominant as-quenched carbides with few ε'-carbides retained after auto-tempering; however, in the Base-Cr-Mo-V-Si steel, it has been found that ε'-carbides occupy a larger number percentage compared to cementite.

(a) 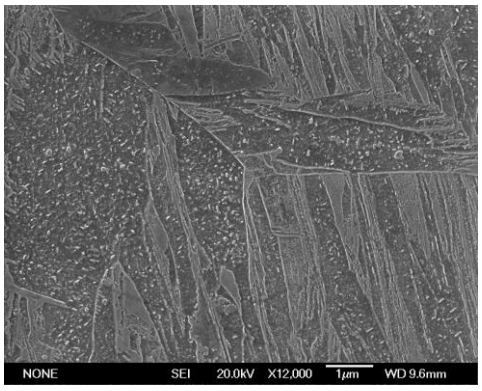

(b) 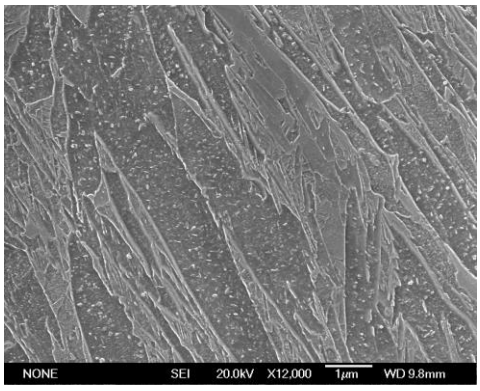

(c) 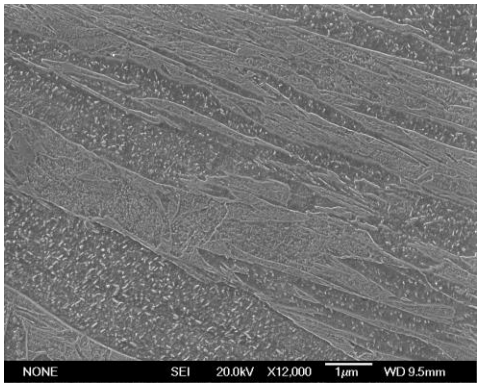

Figure 1. SEM images showing as-quenched carbides present in the martensite laths: (a) Base steel; (b) Base-Mo-V steel; (c) Base-Cr-Si-Mo-V steel.

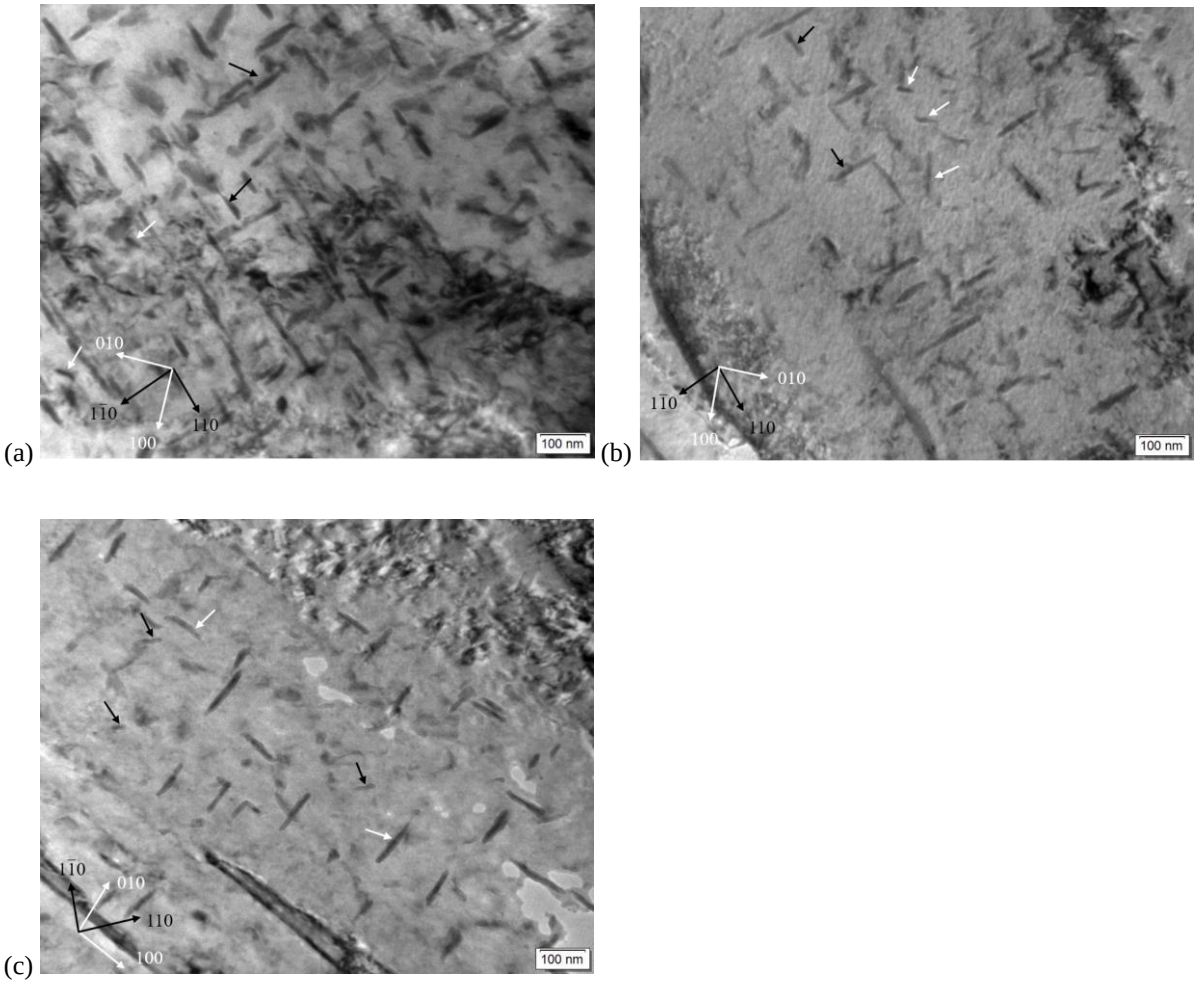

Figure 2. TEM images (<001>α beam direction with in-plane directions on each image) showing needle / plate-shaped carbides present within the as-quenched martensite laths from <001>α beam direction: (a) Base steel; (b) Base-Mo-V steel; (c) Base-Cr-Mo-V-Si steel. The black arrows indicate cementite, whereas the white arrows indicate ε'-carbide.

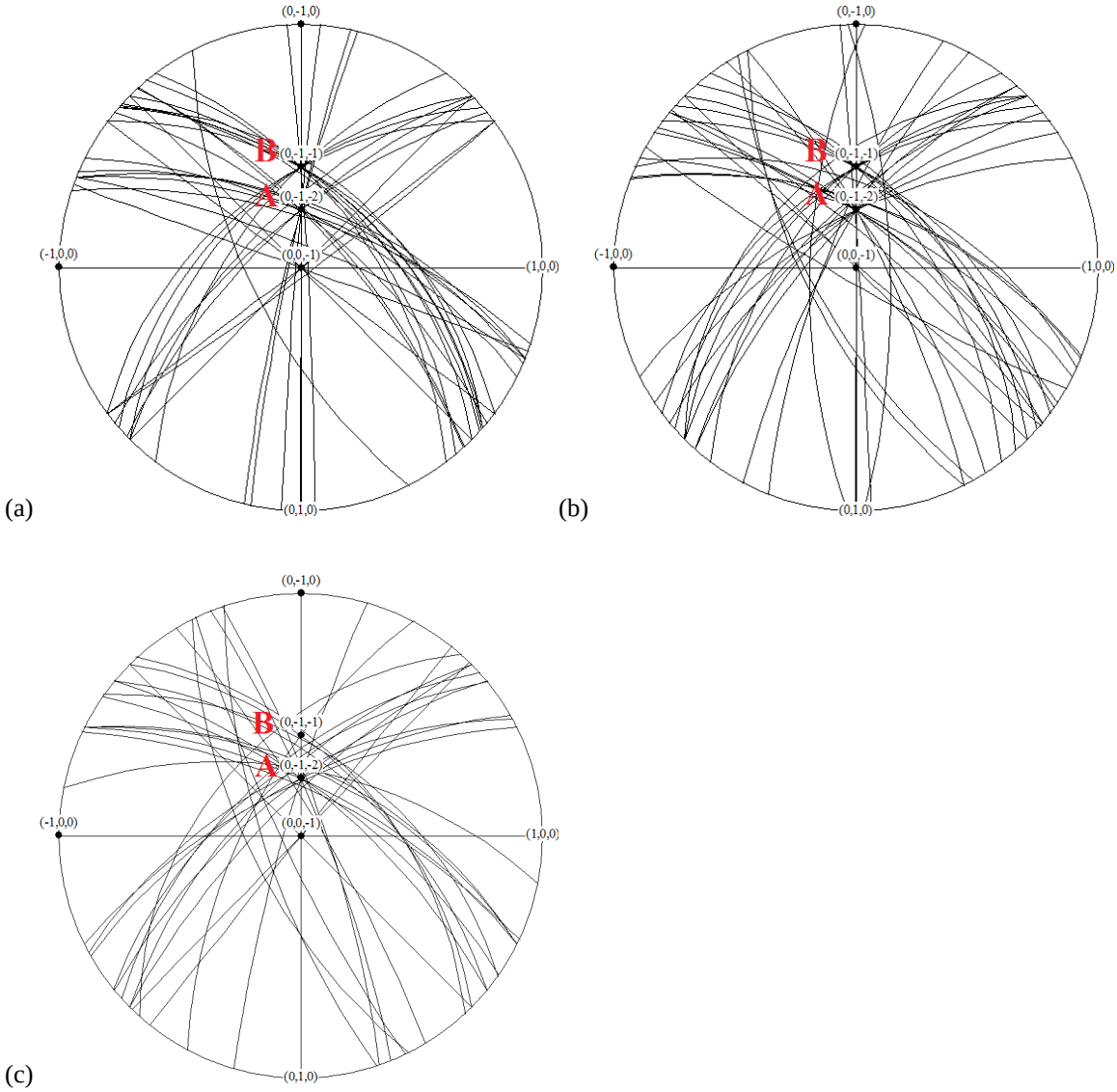

Figure 3. Stereograms indicating the habit planes for the auto-tempered carbides formed during quenching for the three steels: (a) Base steel; (b) Base-Mo-V steel;(c) Base-Cr-Mo-V-Si steel. The intersections A and B in the stereograms refer to {012}α and {011}α poles respectively.

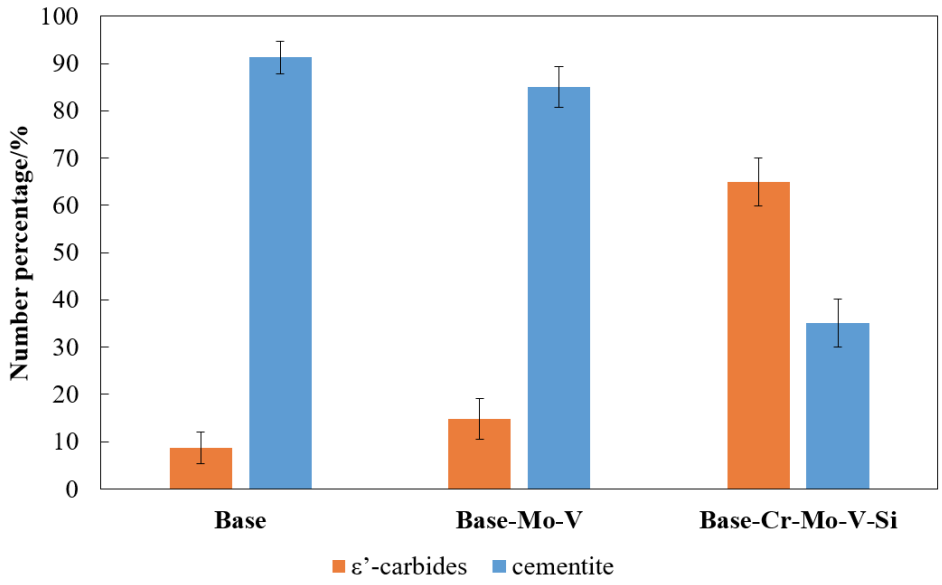

Figure 4. The number percentages of cementite and ε'-carbide in the as-quenched condition in the three steels.

As the martensitic matrix has auto-tempered, the matrix would be expected to be more body centred cubic than body centred tetragonal. The lattice parameter-alloying compositions equation (Equation (1)), derived by Bhadeshia [32] for bcc ferrite, has been used to determine the amount of carbon retained in solid solution after water quenching:

$$a_{BCC} = 0.28664 + (3a_{Fe}^2)^{-1} \times [(a_{Fe} - 0.0279x_C^{\alpha})^2(a_{Fe} + 0.2496x_C^{\alpha}) - a_{Fe}^3] - 0.003x_{Si}^{\alpha} + 0.006x_{Mn}^{\alpha} + 0.007x_{Ni}^{\alpha} + 0.031x_{Mo}^{\alpha} + 0.005x_{Cr}^{\alpha} + 0.0096x_V^{\alpha} \quad (1)$$

Where a_{BCC} is the measured lattice parameter in the three steels, Table 2, a_{Fe} is the lattice parameter of pure ferrite (0.28664 nm [33]); x_i^{α} represents the mole fraction of species i in solution in the matrix. The amount of carbon trapped in solid solution after quenching in the Base and Base-Mo-V steels is similar, Table 2, which is slightly lower than that in the Base-Cr-Mo-V-Si steel consistent with the effect of Si in slowing down carbon diffusion to form carbides during auto-tempering. In addition, the retained carbon content after tempering for 2 hrs in the Base steel has been assessed to be 0.04 wt %, which is much smaller than that in the as-quenched condition, Table 2.

Table 2. Lattice parameters and retained carbon contents in the matrix for the three steels

	Lattice parameter/nm	Carbon content in the matrix (/weight percentage)
Base (As-quenched)	0.28702	0.11
Base-Mo-V (As-quenched)	0.28712	0.11
Base-Cr-Mo-V-Si- (As-quenched)	0.28717	0.13
Base (2hrs)	0.28679	0.04
Base-equilibrium (Thermo-Calc)	-	0.03

(2) Carbide precipitation and coarsening during tempering at 600 °C

As shown in Figure 5, the inter- and intra-lath carbides (arrowed) are elliptical or even spherical in shape in the Base steel when tempering from 2 hrs to 16 hrs at 600 °C, where the inter-lath carbides constitute most of the carbide volume fraction, Figure 6. These elliptical carbides are consistent with cementite (equilibrium carbide in this steel predicted by Thermo-Calc) [34]. The measured cementite volume fraction from SEM images (where a slight overestimation may be expected due to the etching effect) is consistent with the equilibrium value (2.5 %) in the samples tempered from 2 hrs onwards, Table 3, indicating the occurrence of Ostwald ripening for cementite confirmed as its size increases [34]. As the volume fractions for inter- and intra-lath cementite keep approximately constant with time, whereas the number density of both decreases with time, Figure 6, the coarsening of inter-lath cementite occurs independently from that of intra-lath cementite.

However, in the Base-Mo-V and Base-Cr-Mo-V-Si steels, not only the comparatively large elliptical inter- and intra-lath carbides (yellow arrowed), but also fine needle-shaped and even finer elliptical carbides (red arrowed) exist within the laths during tempering from 2 hrs to 16 hrs at 600 °C, Figure 7. The large elliptical carbides, which are confirmed as cementite, Figure 8 and Figure 9, account for nearly all the carbide volume fraction. In addition, the volume fractions for the large elliptical cementite keep approximately constant with tempering time in the two steels, Table 3, and are similar to the Base steel. The inter-lath cementite constitutes most of the elliptical cementite volume fraction with a constant value, whereas the number density decreases with time, Figure 6, which again indicates that

coarsening of the inter-lath cementite takes place independently from that of the intra-lath cementite.

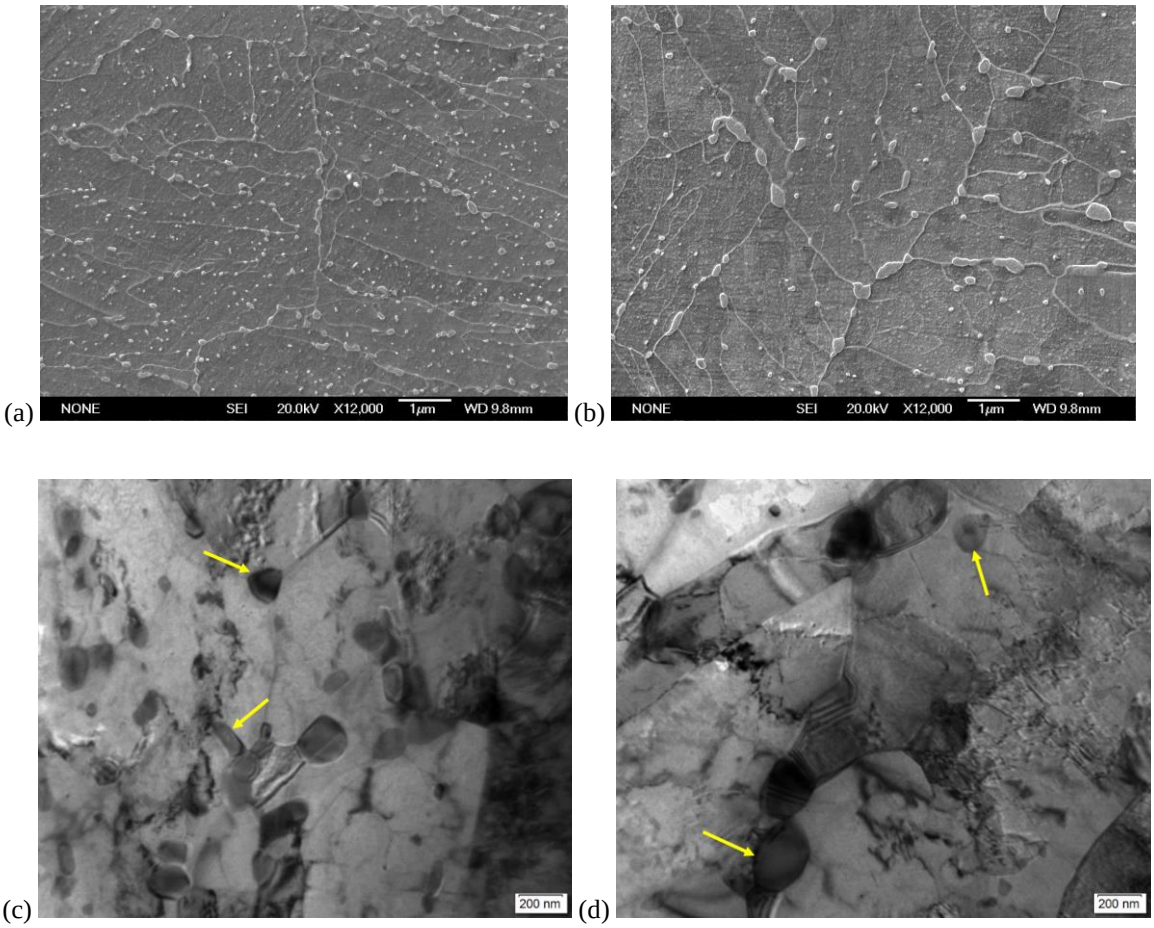

Figure 5. The morphology of carbides after tempering at 600 °C for different times in the Base steel: (a-SEM/c-TEM) 2 hrs; (b-SEM/d-TEM) 16 hrs.

(a)

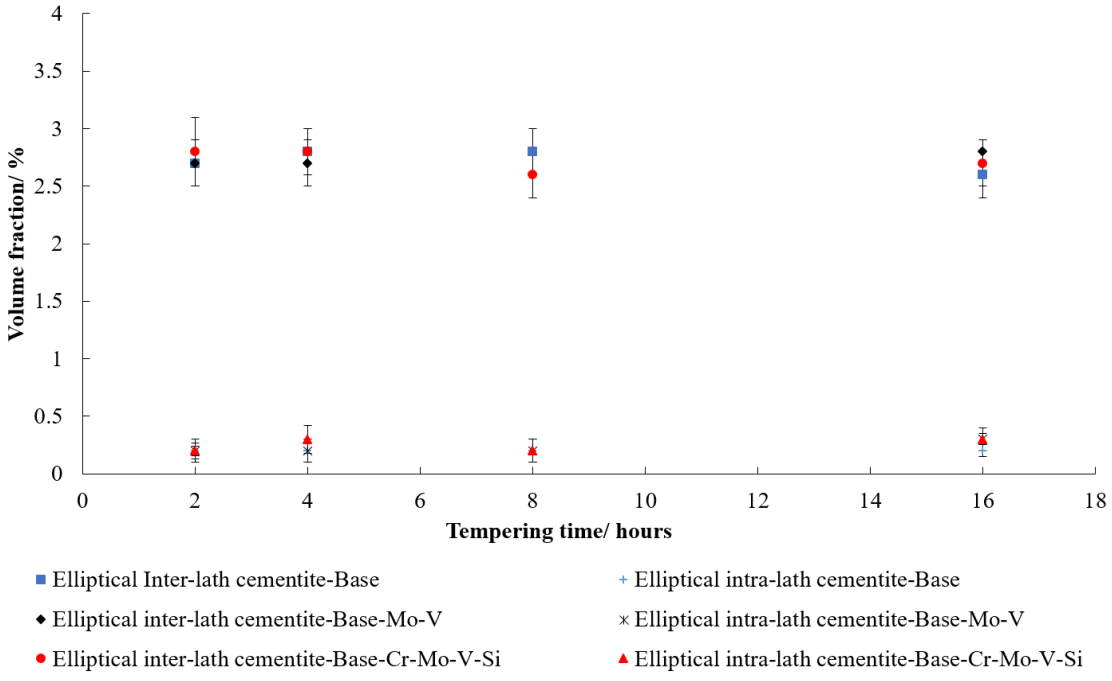

(b)

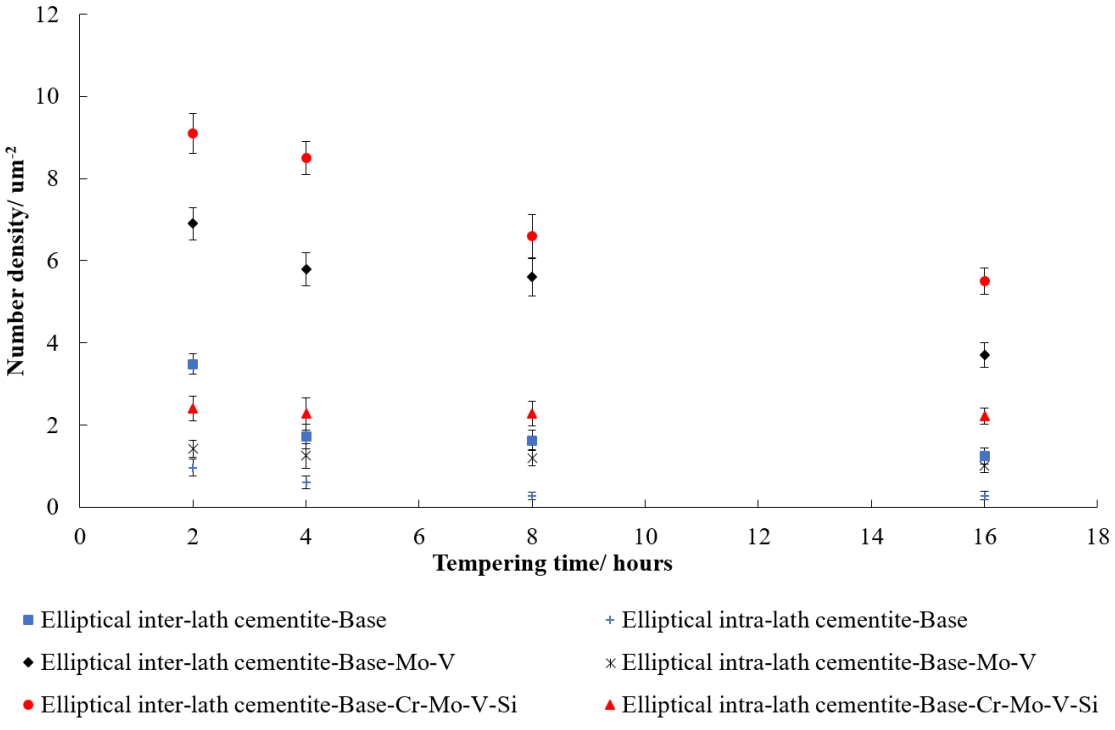

Figure 6. Volume fraction (a) and number density (b) for the elliptical inter- and intra-lath cementite in the three steels during tempering from 2 hrs to 16 hrs at 600 °C (SEM measurements).

Table 3. The elliptical cementite volume fractions in the three steels tempered from 2 hrs to 16 hrs at 600 °C

	2 hrs/ %	4 hrs/ %	8 hrs/ %	16 hrs/ %
Base	2.9±0.3	3.0±0.5	3.0±0.5	2.8±0.4
Base-Mo-V	2.9±0.4	2.9±0.3	2.8±0.3	3.1±0.5
Base-Cr-Mo-V-Si	3.0±0.6	3.1±0.4	2.8±0.2	3.0±0.3

(a) 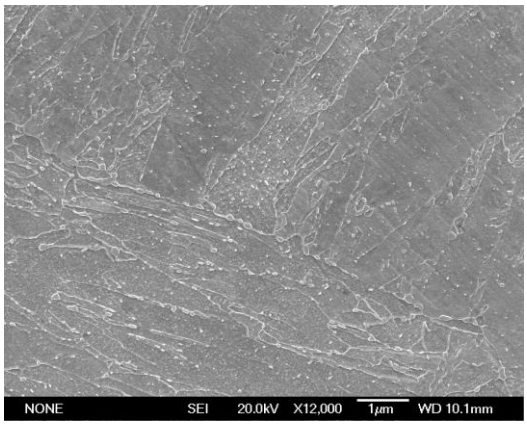

(b) 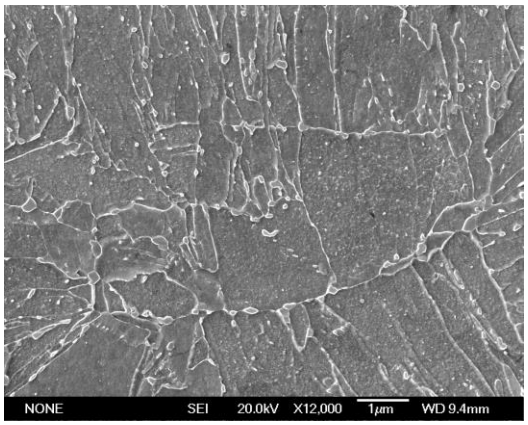

(c) 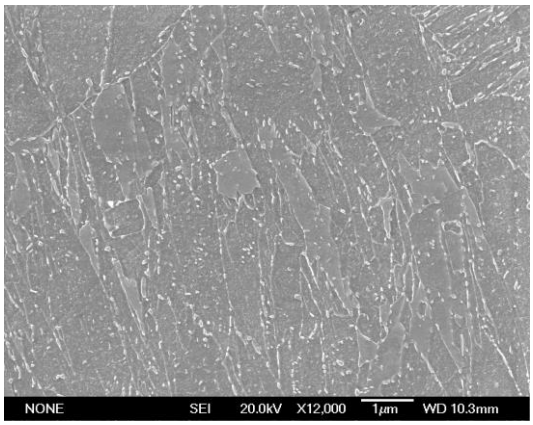

(d) 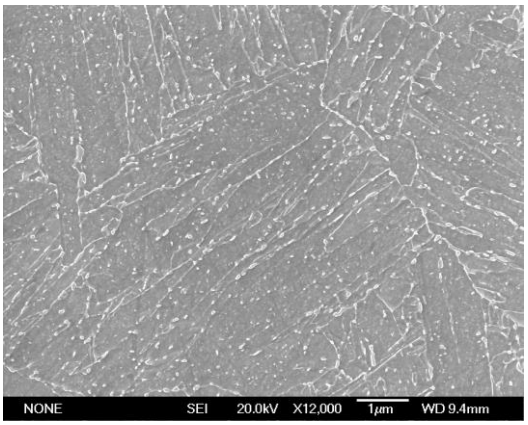

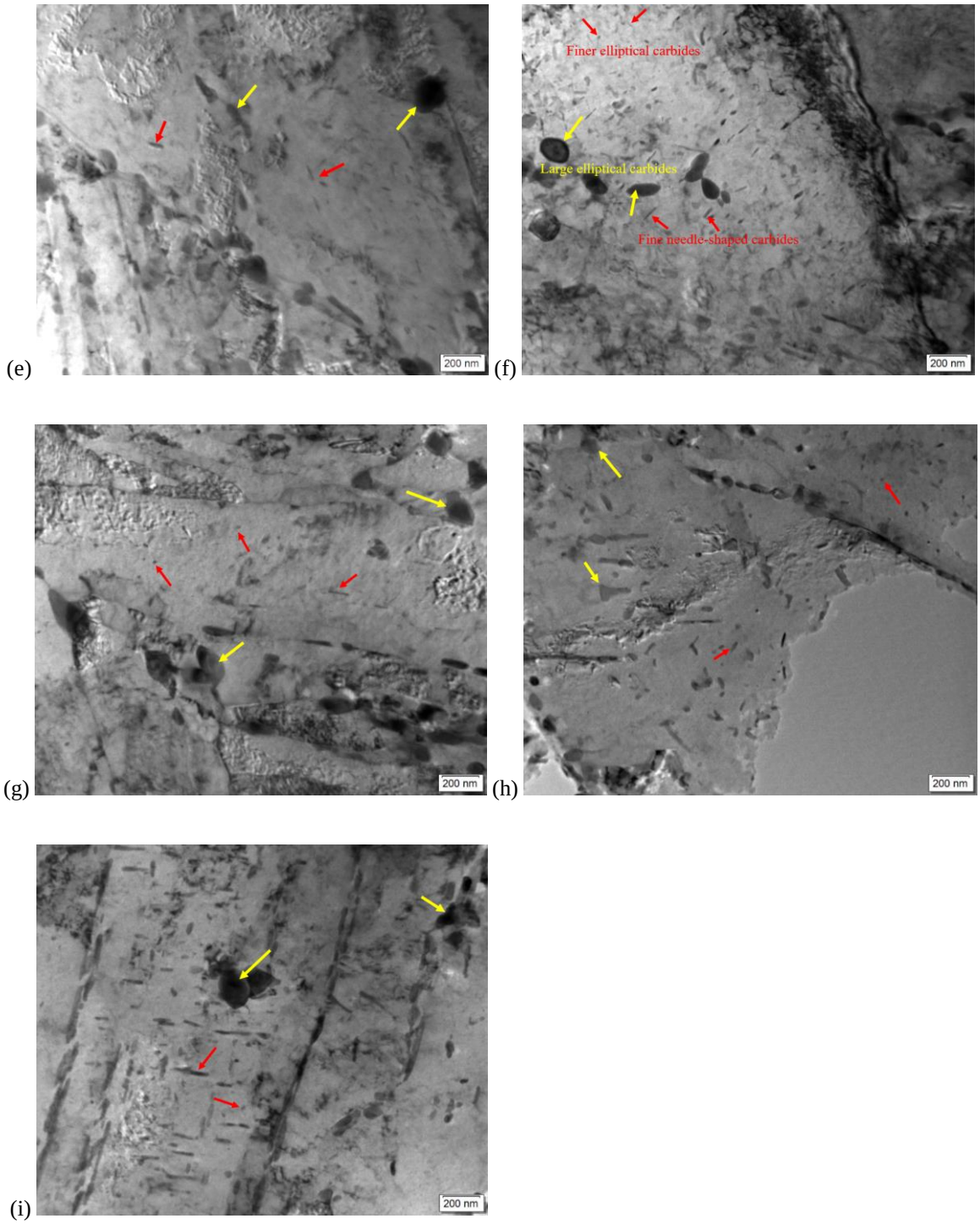

Figure 7. The morphology of carbides after tempering at 600 °C for different times in the Base-Mo-V (a-SEM/e-TEM) 2 hrs, (f-TEM) 4 hrs, (b-SEM/g-TEM)16 hrs and Base-Cr-Mo-V-Si steels (c-SEM/h-TEM) 2hrs, (d-SEM/i-TEM) 16 hrs. The yellow arrows indicate the relatively large inter- / intra-lath cementite, and the red arrows indicate the needle-shaped carbides and finer elliptical carbides within the laths in the two steels.

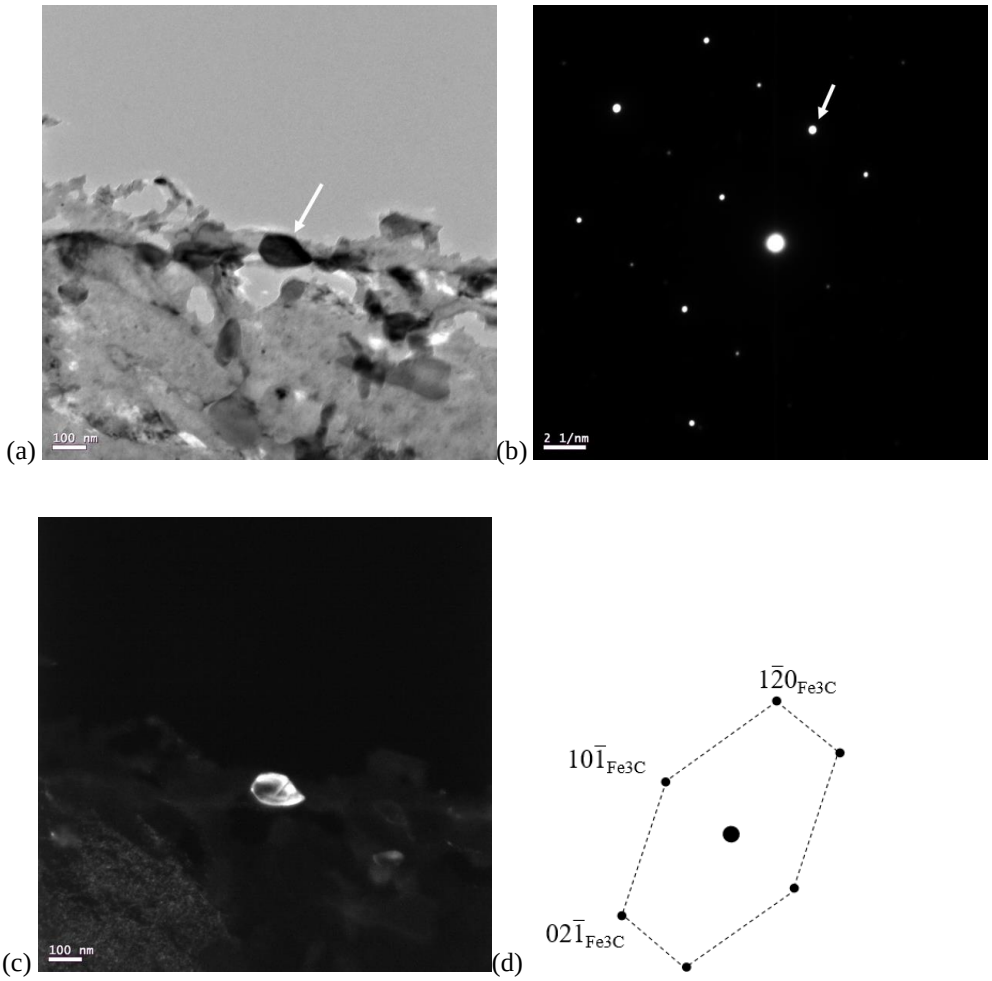

Figure 8. Characterisation of elliptical carbides after tempering for 2 hrs at 600 °C in the Base-Mo-V steel: (a) Bright field image of a typical elliptical carbide; (b) SAD pattern for the particle consistent with the [212] zone axis of cementite as shown in (d); (c) Dark field image with the diffracted spot (arrowed in (b)) selected.

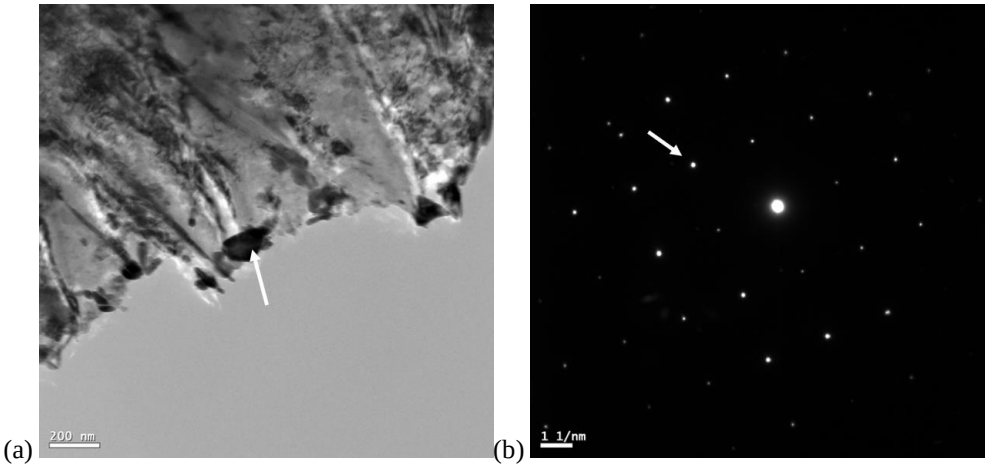

(c) 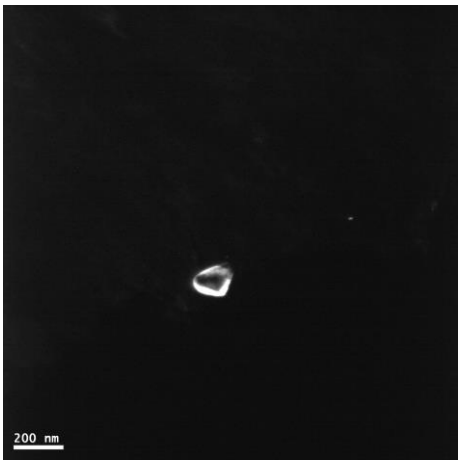

(d) 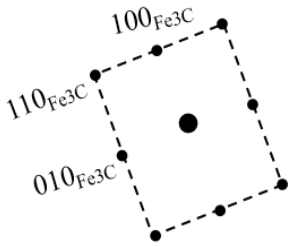

Figure 9. Characterisation of elliptical carbides after tempering for 2 hrs at 600 °C in the Base-Cr-Mo-V-Si steel: (a) Bright field image of a typical elliptical carbide; (b) SAD pattern for the particle consistent with the [00-1] zone axis of cementite as shown in (d); (c) Dark field image of the elliptical carbide with the diffracted spot (arrowed in (b)) selected.

The carbide-forming elements can enrich cementite during tempering at relatively high temperatures [3, 16, 17], thus, the chemical compositions for the large elliptical cementite particles in the three steels have been measured and compared with Thermo-Calc calculations, Figures 10 - 12 and Table 4. In the Base steel, the equilibrium carbide is predicted to be cementite, whereas cementite and M_2C carbide are predicted as the pseudo-equilibrium carbides in the Base-Mo-V and Base-Cr-Mo-V-Si steels. In order to consistently check the substitutional element contents in different carbides / matrix, the substitutional element M (M= Mn, Mo, V and Cr) to Fe ratio Y_M is used as defined in Equation (2):

$$Y_M = wt\ (M) / wt\ (Fe) \quad (2)$$

Where *wt* (M) and *wt* (Fe) are the weight percentages of M and Fe respectively from the EDS measurements. As listed in Table 4, the substitutional elements, such as Mn, Mo, Cr and V, enrich the elliptical cementite particles in the three steels during tempering at 600 °C, as reported in other systems [3, 16, 17], which is approximately consistent with the Thermo-Calc prediction in that clear enrichment of Mn, Mo and Cr is seen. The values are lower than predicted for the major elements of Mn and Cr which may be due to experimental errors and/or insufficient time for the equilibrium levels to be reached. However, the presence of the alloying elements in the cementite particles means that it is their diffusion which will dominate the coarsening of the elliptical inter- / intra-lath cementite. Si is depleted in cementite and partitioned into the matrix, as no or a very weak peak is found in the EDS

spectra for cementite particles, which agrees well with reports in the literature for Si-enriched steels, e.g. Fe-0.6C-2Si steel [16].

(a)

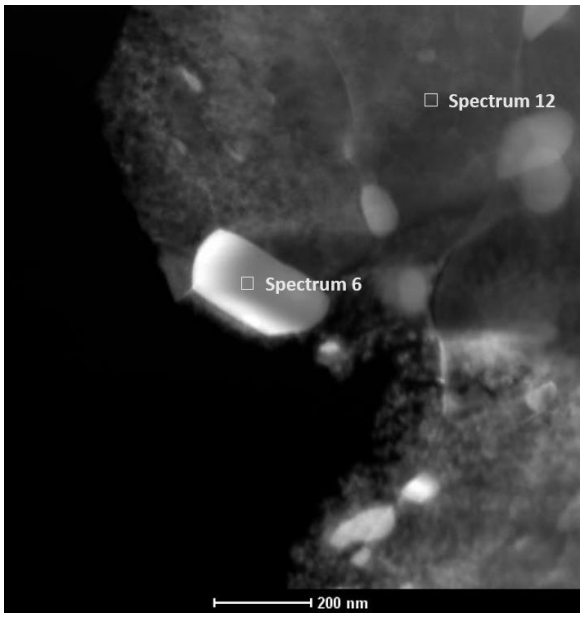

(b)

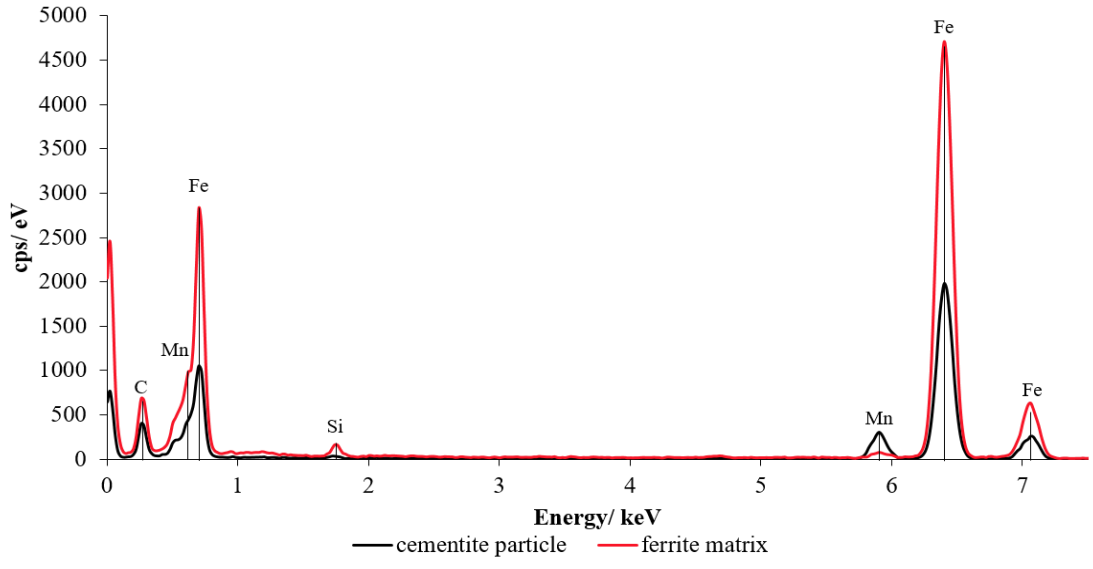

Figure 10. The chemical compositions for cementite and the ferrite matrix in the Base steel after tempering for 2 hrs from EDS measurements using a thin foil specimen: (a) the morphology of the selected particle and matrix for EDX measurements; (b) EDX spectra for the cementite particle and ferrite matrix.

(a)

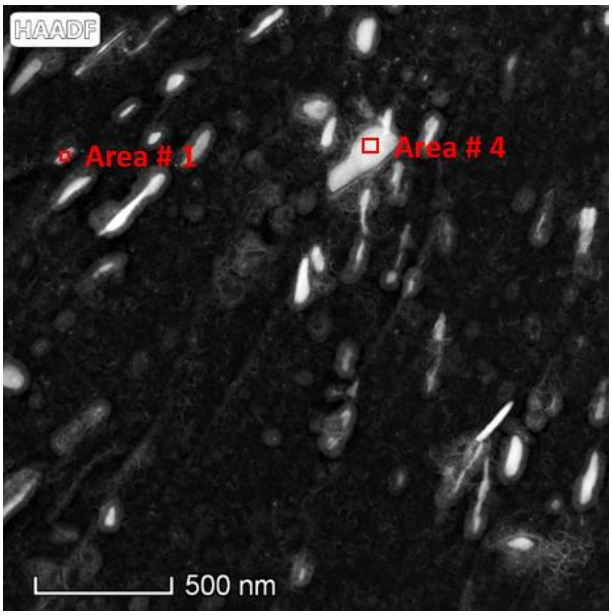

(b)

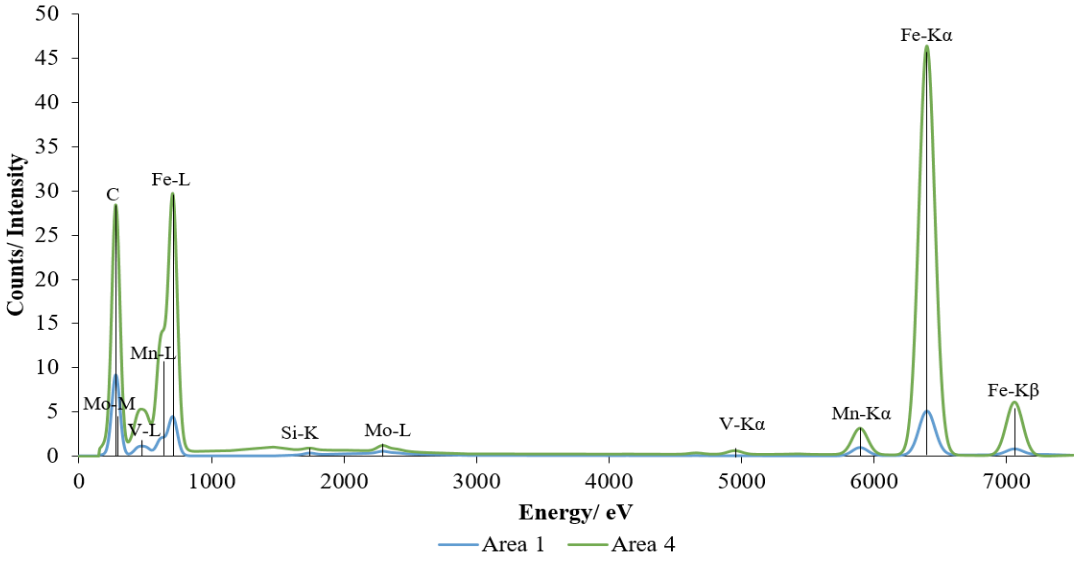

Figure 11. The chemical composition for cementite in the Base-Mo-V steel after tempering for 2 hrs from EDS measurements using a carbon replica specimen: (a) the morphology of the selected particles for EDX measurements; (b) EDX spectra for the fine needle-shaped particle (Area 1) and elliptical cementite particle (Area 4).

(a)

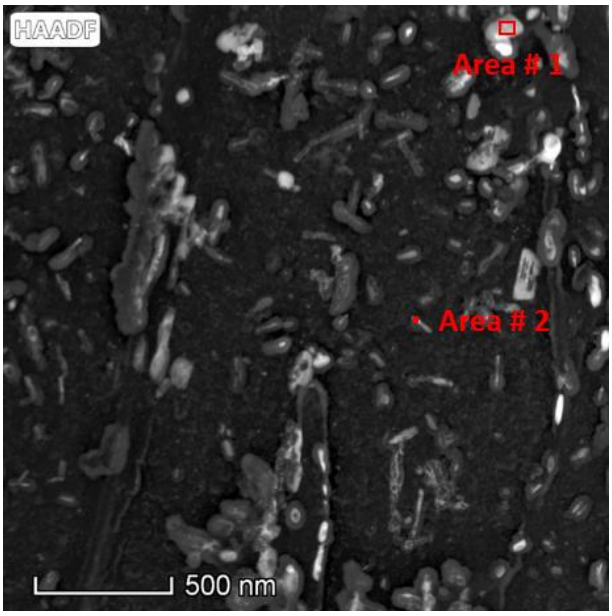

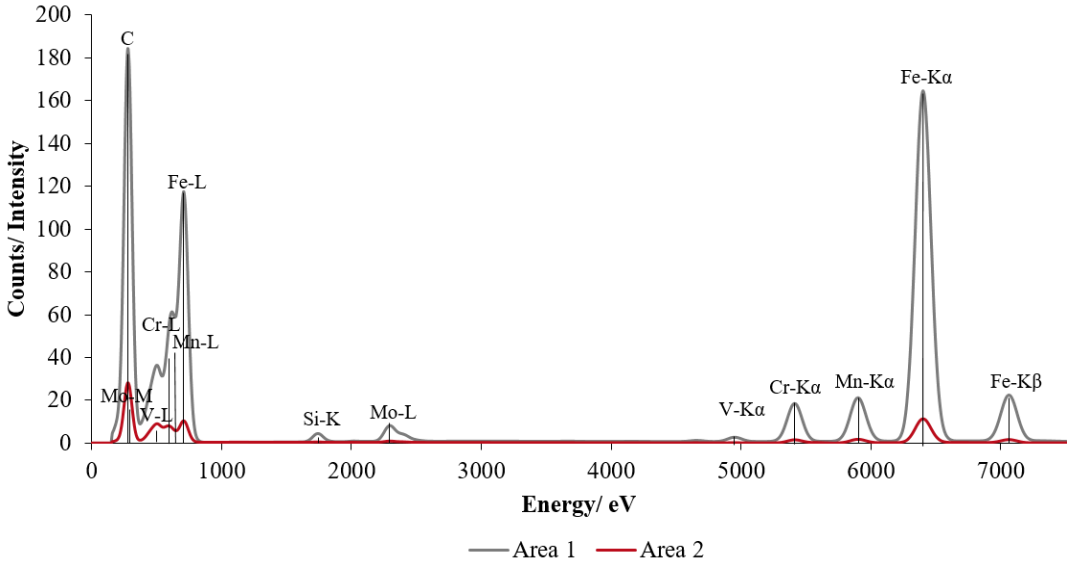

(b)

Figure 12. The chemical composition for cementite in the Base-Cr-Mo-V-Si steel after tempering for 2 hrs from EDS measurements using a carbon replica specimen: (a) the morphology of the selected particles for EDX measurements; (b) EDX spectra for the elliptical cementite particle (Area 1) and fine needle-shaped particle (Area 2).

Table 4. The M to Fe ratio Y_M (M = Mn, Cr, Mo and V) for different particles and the ferrite matrix in Figure 10 - Figure 12 from the EDS measurements in the three steels after tempering for 2 hrs at 600 °C and compared with the Thermo-Calc prediction

	Y_{Mn}	Y_{Mo}	Y_V	Y_{Cr}
Base - elliptical cementite particle	0.14	-	-	-
Base - matrix	0.01	-	-	-
Base-equilibrium cementite (Thermo-Calc)	0.19			
Base-Mo-V - elliptical cementite particle	0.09	0.02	0.01	-
Base-Mo-V - fine needle-shape particle	0.11	0.02	0.01	-
Base-Mo-V-pseudo-equilibrium cementite (Thermo-Calc)	0.17	0.01	0.00	
Base-Cr-Mo-V-Si - elliptical cementite particle	0.09	0.03	0.01	0.08
Base-Cr-Mo-V-Si - fine needle-shaped particle	0.11	0.04	0.01	0.11
Base-Cr-Mo-V-Si-pseudo-equilibrium cementite (Thermo-Calc)	0.17	0.03	0.00	0.29

In addition, very fine carbides, including needle-shaped and elliptical-shaped carbides (arrowed in Figure 7), also appear within the martensite laths in the Base-Mo-V and Base-Cr-Mo-V-Si steels during tempering from 2 hrs to 16 hrs at 600 °C, although they are not seen in the Base steel. The number density variation for these fine carbides in the two steels is shown in Figure 13. The number density initially decreases during tempering from 0 hr to 2 hrs, and the fine needle-shaped carbides present after tempering for 2 hrs are consistent with being cementite, as their chemical composition is very similar to that for the elliptical cementite, Figure 11, Figure 12 and Table 4. Besides, no alloy carbides (such as M_2C type Mo-rich carbides) are detected in the two steels in the 2 hour tempered condition. However, with the tempering time extending from 2 hrs to 4 hrs, the number density of fine carbides increases in the two steels, Figure 13, indicating precipitation of secondary hardening alloy carbides, as the number density attributed to fine needle-shaped cementite should decrease with time as coarsening progresses. An additional distribution of finer elliptical alloy carbides are

observed in the TEM samples after tempering for 4 hrs, whose chemical composition is obviously different from that for cementite: the Y_{Mo} and Y_V values in these finer elliptical carbides are several hundreds of times larger than those in cementite, Figure 14 and Table 5. Actually, the measured Y_{Mo}, Y_V and Y_{Mn} in these finer elliptical alloy carbides are quite different from the predicted composition for the pseudo-equilibrium M_2C carbides (Thermo-Calc), predominantly due to the precipitation of these finer elliptical alloy carbides not achieving the pseudo-equilibrium condition after tempering for 4 hrs in the two steels. This additional set of carbides explains the increase in number density observed for fine carbides tempered from 2 hrs to 4 hrs in Figure 13 and are expected to be Mo-V-rich M_2C carbides, as M_2C carbides have been reported to form after cementite in a Fe-0.6Cr-0.5Mo steel [23] or Cr-Mo-V steels with low V/Mo ratio (< 0.17) [24] during the early stage of tempering. As the tempering time increases from 4 hrs to 16 hrs, the number density for the fine carbides decreases, indicating the continuous dissolution of fine needle-shaped cementite as cementite coarsening proceeds and the gradual growth of the secondary alloy carbides in the two steels. The number density of fine carbides in Base-Cr-Mo-V-Si steel is slightly higher than in Base-Mo-V steel, Figure 13, consistent with the higher content of Si retarding the dissolution of the needle-shaped cementite.

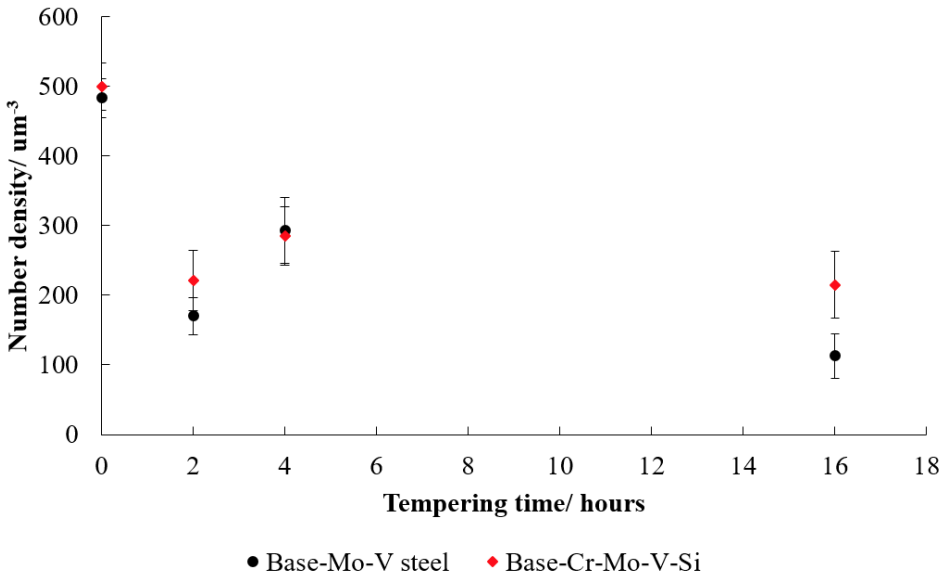

Figure 13. The number density variation for very fine carbides (including needle-shaped and finer elliptical carbides) in the Base-Mo-V and Base-Cr-Mo-V-Si steels (TEM measurements).

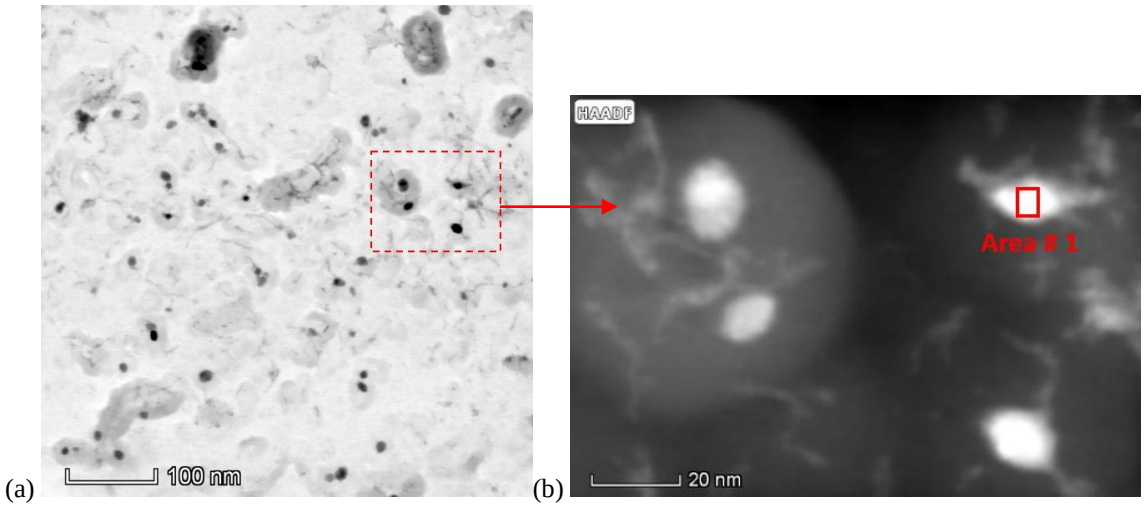

(a) (b)

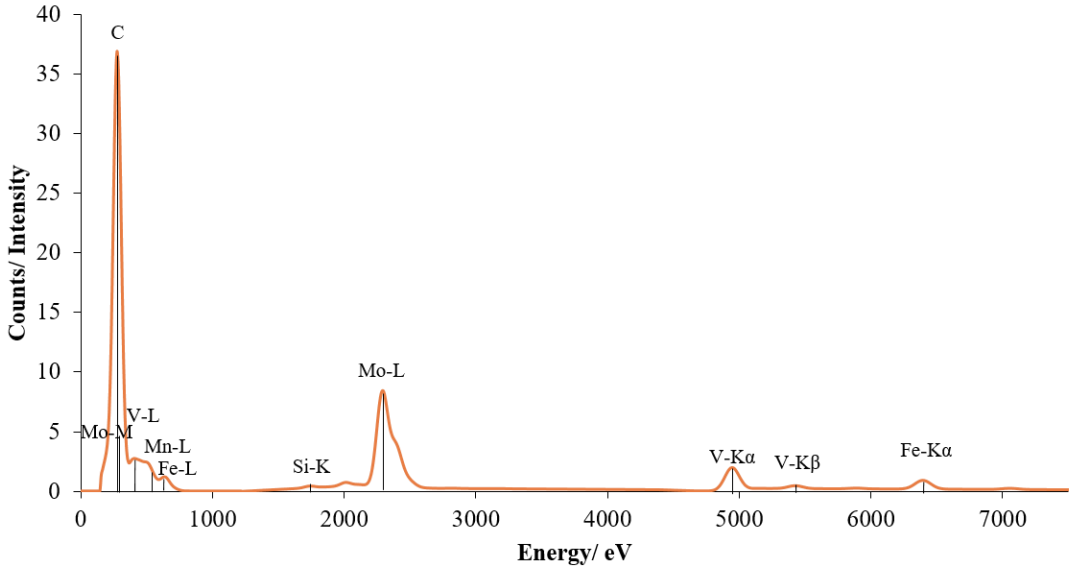

(c)

Figure 14. The chemical composition for secondary alloy carbide in the Base-Mo-V steel after tempering for 4 hrs from EDS measurements using a carbon replica specimen: (a), (b) the morphology of the selected particle for EDX measurements; (c) EDX spectrum for the finer elliptical carbide.

Table 5. The M (Mn, Mo and V) to Fe ratio Y_M for the analysed carbide in Figure 14 in the Base-Mo-V steel after tempering for 4 hrs at 600 °C and compared with the Thermo-Calc prediction

	Y_{Mn}	Y_{Mo}	Y_V
Base-Mo-V- finer elliptical particle	0.08	14.75	2.13
Base-Mo-V-pseudo-equilibrium M_2C carbide (Thermo-Calc)	7.07	55.96	3.04

Discussion

Auto-tempering occurs in the three steels during water quenching, where cementite and ε'-carbide are both observed, in contrast with some reports for these grades [1-4]. In the Base and Base-Mo-V steels, the dominant as-quenched carbide is cementite. As the carbon diffusion distance has been estimated to be 90 nm for cooling from the ε'-carbide formation temperature [34], it is feasible for cementite to form on the pre-existing ε'-carbides, which is consistent with the measured carbide spacing of approximately 100±50 nm in the two steels. The formation of cementite can be significantly suppressed with Si contents exceeding 1.4 wt % in steels [9], and it has been found that, in the Base-Cr-Mo-V-Si steel, ε'-carbide is the predominant as-quenched carbide, Figure 4, which is consistent with the extra addition of Si delaying the transformation from ε'-carbide to cementite during auto-tempering [10]. The retained carbon contents in the Base and Base-Mo-V steels remain constant after water quenching, Table 2, resulting in a similar hardness in the as-quenched condition for the two steels (458±12 HV for the Base steel, 454±11 HV for the Base-Mo-V steel). However, a slightly higher retained carbon content as well as alloying contents (such as Cr and Si) are present in the Base-Cr-Mo-V-Si steel, which leads to a little bit higher as-quenched hardness being observed (471±12 HV) in this steel. Therefore, it is expected that carbon will continue to come out of solid solution in the three steels, probably diffusing to pre-existing carbides causing growth, during tempering from 0 hr to 2 hrs at 600 °C. In the Base steel, the retained carbon content in solid solution decreases on tempering from 0 hr to 2 hrs and nearly achieves the equilibrium carbon content after tempering for 2 hrs, Table 2. The reduction of retained carbon content is predicted to lead to an approximately 200 HV hardness decrease based on the hardness - carbon content relationship [35] as carbon significantly contributes to solid solution strengthening. This is consistent with the significant hardness drop measured for the Base steel tempered from 0 hr to 2 hrs, where the hardness changes from 458±12 HV (as-quenched condition) to 263±3 HV (after tempering for 2 hrs).

In the Base steel, Ostwald ripening of cementite occurs as the carbide sizes increase (Figure 15) during tempering from 2 hrs to 16 hrs, where coarsening of inter-lath cementite with a larger size takes place independently from that of intra-lath cementite. Therefore, the solute diffusion in this steel is either along the lath boundary or through the bulk between cementite particles, not through the bulk to a boundary during this early stage of tempering [34]. The precipitation sequence in this steel is cementite + ε'-carbides → cementite →independent

coarsening of inter / intra-lath cementite. As coarsening of cementite occurs when tempering from 2 hrs to 16 hrs, a continuous hardness decrease is estimated to be approximately 24 HB (≈ 24 HV) based on the Hírsch and Humphreys precipitation hardening equation [36], Figure 16, which is less than the actual hardness decrease (around 40 HV in Figure 17). The equation may be under predicting the effect of the change in size and number density of carbides on hardness, as the precipitation hardening equation was developed for a uniform distribution of a single size distribution of precipitates, whereas the inter-lath and intra-lath elliptical cementite in the Base steel are different populations (i.e. different size distributions) and are not uniformly distributed (particularly for the inter-lath cementite).

In the Base-Mo-V and Base-Cr-Mo-V-Si steels, the stable volume fraction for the large elliptical cementite is also established during tempering from 2 hrs to 16 hrs, Table 3, where the inter-lath cementite also occupies the majority of the cementite volume fraction, Figure 6, being consistent with the Base steel. The coarsening of cementite occurs as its size increases, Figure 15, where again the coarsening of inter-lath cementite takes place independently from that of intra-lath cementite in the two steels. However, the rates of coarsening for the elliptical inter- / intra-lath cementite in the three steels differ and rank as Base> Base-Mo-V> Base-Cr-Mo-V-Si, Figure 15, due to the different diffusivities of substitutional elements that are partitioning into cementite during tempering as well as any effects of Si in the matrix. The rate of coarsening for the elliptical cementite in the Base-Mo-V steel is much lower than that in the Base steel due to its higher content of alloying elements (Mo and V). Normally, Mo has a smaller diffusivity compared to Mn in the ferrite matrix (D_{Mo}= 4.2×10^{-19} m^2/s and D_{Mn}=2.6×10^{-18} m^2/s in ferrite at 600 °C [37]), therefore, the cementite coarsening rate in the Base-Mo-V steel is reduced compared to that in the Base steel. In the Base-Cr-Mo-V-Si steel, the spheroidisation and coarsening of cementite is even more inhibited with the extra addition of Si, where a finer dispersion of cementite is observed in Figure 7 (c) (d). In addition, the sizes for the elliptical inter-lath cementite are obviously larger than those for intra-lath cementite in the three steels due to faster solute lath/grain boundary diffusion [38, 39], Figure 15, being consistent with observations made in Fe-0.1C-1.99Mn-1.60Mo steel [22] or Fe-0.45C-0.22Si-0.62Mn-0.004P-0.0038S steel [20, 21]. As secondary Mo-V-rich carbides are observed after tempering for 4 hrs in the Base-Mo-V and Base-Cr-Mo-V-Si steels, hence, the precipitation sequence for the two steels is cementite + ε'-carbide → cementite → secondary Mo-V-rich (expected to be M_2C) carbides + independent coarsening of inter- / intra-lath cementite at a lower coarsening rate than the Base steel. Therefore, solute diffusion in the

Base-Mo-V and Base-Cr-Mo-V-Si steels is either along the lath boundary resulting in coarsening of the inter-lath cementite, or through the bulk leading to coarsening of the intra-lath cementite and formation of secondary Mo-V-rich carbides during the early stage of tempering.

In the Base-Mo-V and Base-Cr-Mo-V-Si steels, the hardness results are approximately the same during tempering from 2 hrs to 16 hrs, Figure 17, and remain 100 HV higher than that in the Base steel probably due to the existence of the fine carbides (needle-shaped cementite or/and secondary alloy carbides). The hardness decrease in the two steels (around 40 HV) is similar to that in the Base steel on tempering from 2 hrs to 16 hrs, where coarsening of the elliptical cementite in the two steels is estimated to contribute about 17 HB (≈17 HV) to the hardness decrease using the Hírsch and Humphreys precipitation hardening equation [36], Figure 16. In addition, it is interesting to note that the observation of fine secondary alloy carbides (M_2C) after 4 hours tempering does not appear to result in any secondary hardening peak in the two steels, which is consistent with 0.1C-0.47Mo or 0.35C-0.5Cr steels [40, 41] where there is no significant secondary hardening peak present during tempering. This may be due to the low level of alloying content used (0.5 wt % Mo) resulting in only a small increase in overall number density of fine carbides, Figure 13.

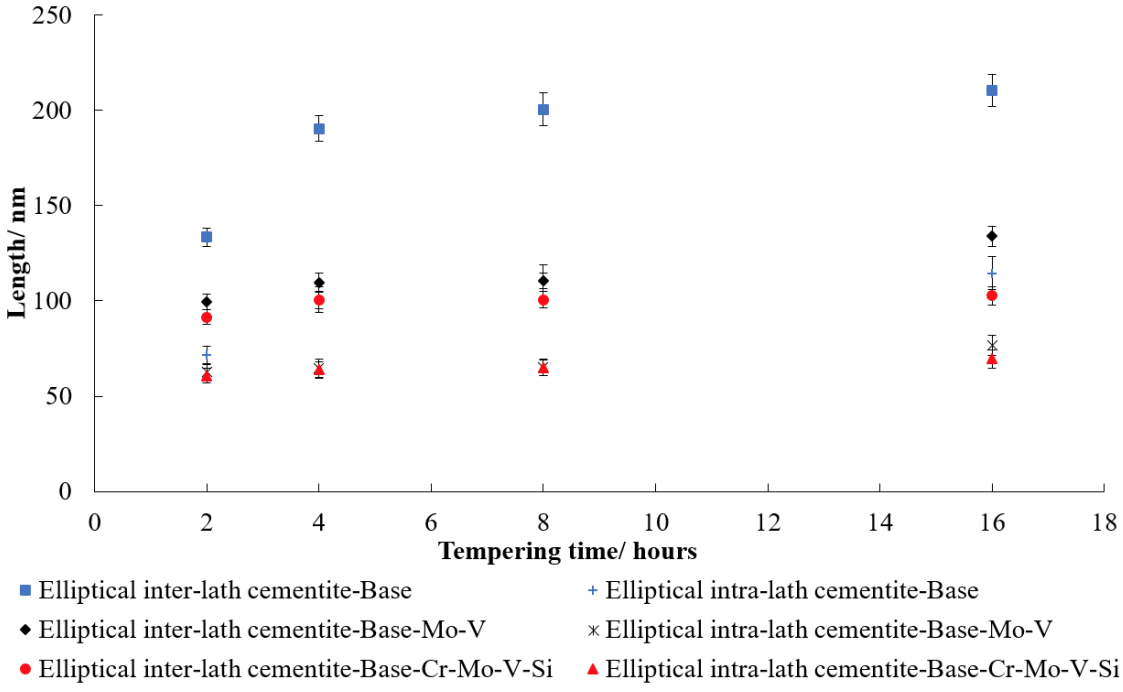

(a)

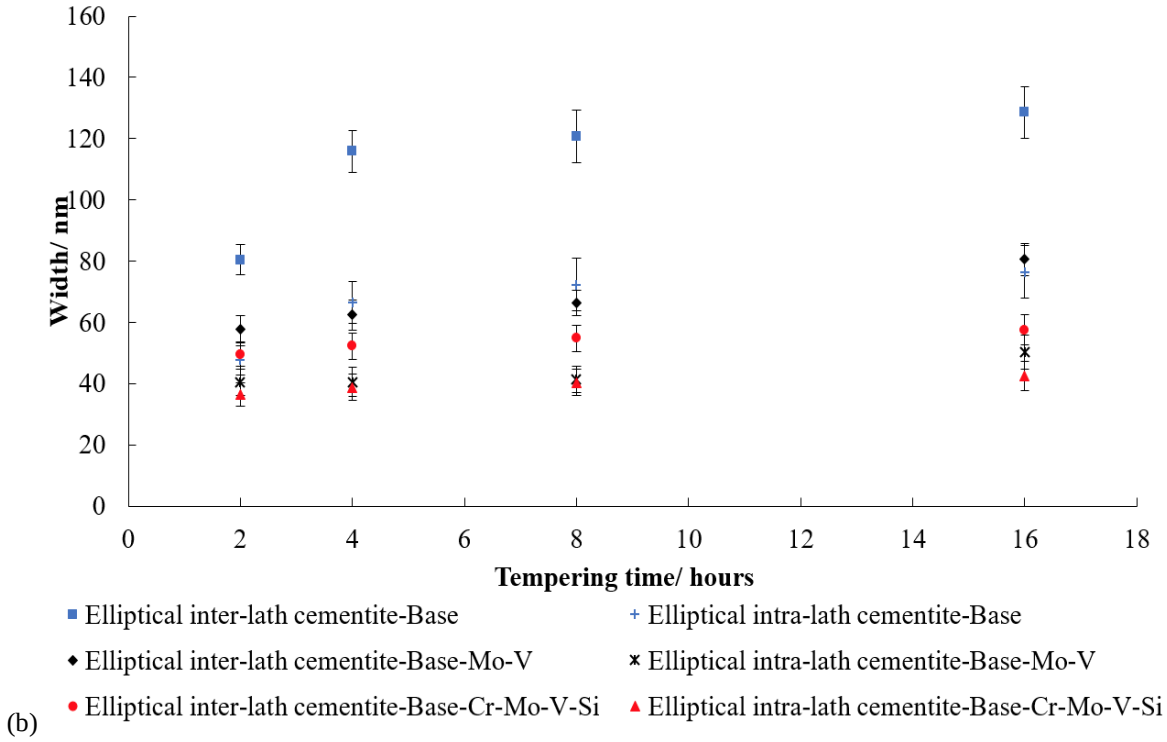

(b)

Figure 15. Average sizes of the elliptical cementite particles after tempering from 2 hrs to 16 hrs at 600 °C in the three steels: (a) length; (b) width.

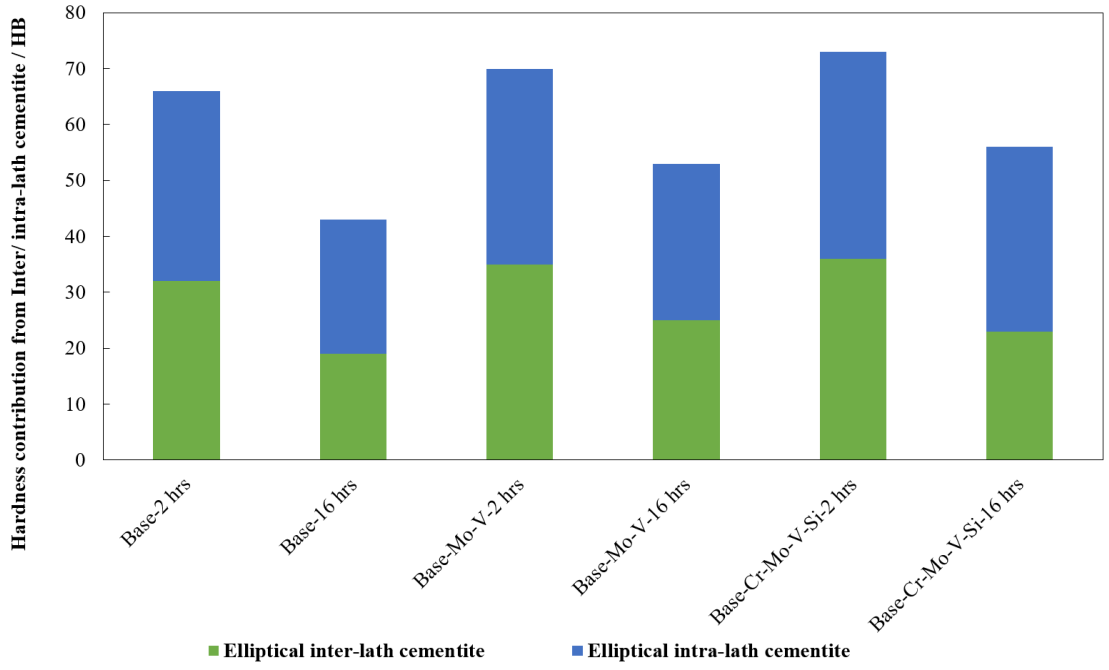

Figure 16. Predicted (using Hírsch and Humphreys precipitation hardening equation [36]) elliptical inter- / intra-lath cementite contribution to hardness in the three steels after tempering for 2 hrs and 16 hrs at 600 °C.

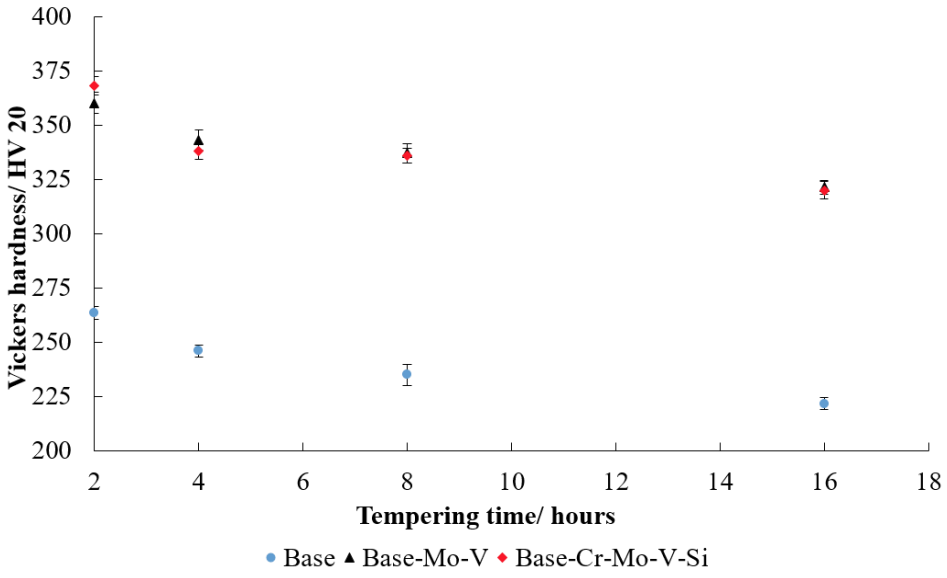

Figure 17. Hardness variation with time in the three steels during tempering from 2 hrs to 16 hrs at 600 °C.

Conclusions

The carbide precipitation and coarsening behaviours related with hardness variation in low carbon low alloy Q&T steels have been quantified, where the effect of alloying elements (Mo, V, Cr and Si) on the tempering response has been considered during the early stages of tempering. It has been determined that coarsening of cementite dominates the behaviour but that coarsening of inter-lath and intra-lath cementite occurs independently in the three steels. Based on the carbide characterisation and hardness analysis, the main conclusions are:

(1) Auto-tempering occurs in the three low carbon low alloy Q&T steels during water quenching, where cementite and ε'-carbide are both observed. In the Base and Base-Mo-V steels, cementite is the predominant as-quenched carbide; however, in the Base-Cr-Mo-V-Si steel, ε'-carbide occupies a larger number percentage consistent with the extra addition of Si.

(2) In the Base steel, only elliptical cementite with chemical composition $(FeMn)_3C$ is observed within the laths and on the lath/grain boundaries when tempering from 2 hrs to 16 hrs at 600 °C, during which time coarsening of cementite takes place. The precipitation sequence for this steel is cementite + ε'-carbide → cementite → independent coarsening of inter- / intra-lath cementite.

(3) In the Base-Mo-V and Base-Cr-Mo-V-Si steels, relatively large elliptical inter- / intra-lath cementite and fine needle-shaped cementite within the laths both exist during tempering from

2 hrs to 16 hrs at 600 °C. The chemical compositions for cementite in the Base-Mo-V and Base-Cr-Mo-V-Si steels are $(FeMnMoV)_3C$ and $(FeCrMnMoV)_3C$ respectively. Secondary Mo-V-rich carbides have been firstly observed after tempering for 4 hrs at 600 °C. The precipitation sequence for the two steels is cementite + ε'-carbide → cementite → secondary Mo-V-rich (expected to be $(MoV)_2C$) carbides + independent coarsening of inter- / intra-lath cementite at a lower coarsening rate than the Base steel.

(4) In the three steels, coarsening of cementite contributes to the softening process in the three steels during tempering. The observation of fine secondary Mo-V-rich carbides after 4 hours tempering does not appear to result in any secondary hardening peak in the Base-Mo-V and Base-Cr-Mo-V-Si steels.

Acknowledgements

Thanks are given to the China Scholarship Council (CSC) for financial support for the PhD study of the lead author at the University of Birmingham. Thanks are given to British Steel Ltd and Tata Steel (UK) for the provision of material and technical discussions. Thanks are also given to Siben Jiang in University of Birmingham and Geoff West in University of Warwick for experimental support.

Data availability

The raw/processed data required to reproduce these findings cannot be shared at this time due to legal or ethical reasons.

References

[1] E. R. Parker. Interrelations of compositions, transformation kinetics, morphology, and mechanical properties of alloy steels, Metallurgical Transaction A. 8 (1977) 1025-1042. https://doi.org/10.1007/bf02667387.

[2] S. W. Ooi, Y. R. Cho, J. K. Oh and H. K. D. H. Bhadeshia. Carbon enrichment in residual austenite during martensitic transformation, International Conference on Martensitic Transformations. (2009) 179-185. https://doi.org/10.1002/9781118803592.ch25.

[3] A. J. Clarke, M. K. Miller, R. D. Field, D. R. Coughlin, P. J. Gibbs, K. D. Clarke, D. J. Alexander, K. A. Powers, P. A. Papin, G. Krauss. Atomic and nanoscale chemical and structural changes in quenched and tempered 4340 steel, Acta Materialia. 77 (2014) 17-27. https://doi.org/10.1016/j.actamat.2014.05.032.

[4] J. Gallego, A. R. Rodrigues, C. L. F. d. Assis, L. Montanari. Second phase precipitation in ultrafine-grained ferrite steel, Materials Research. 17 (2014) 527-534. http://dx.doi.org/10.1590/S1516-14392013005000199.

[5] K. H. Jack. Structural transformations in the tempering of high-carbon martensitic steels, Journal of Iron and Steel Institute. 169 (1951) 26-36.

[6] K. A. Taylor, G. B. Olson, M. Cohen, J. B. Vander Sande. Carbide precipitation during stage I tempering of Fe-Ni-C martensites, Metallurgical Transaction A. 20 (1989) 2749-2765. https://doi.org/10.1007/bf02670168.

[7] Y. Ohmori, I. Tamura. Epsilon carbide precipitation during tempering of plain carbon martensite, Metallurgical Transactions A. 23 (1992) 2737-2751. https://doi.org/10.1007/bf02651753.

[8] G. Badinier. Effect of carbon segregation and carbide precipitation on the mechanical response of martensite. PhD thesis, University of British Columbia, 2013.

[9] B. Kim, D. S. Martin, J. Chao, P. E. J .Rivera-Díaz-Del-Castillo. The effect of silicon on the $\varepsilon \rightarrow \theta$ transformation in ultra-strong spring steels, Materials Science and Technology Conference and Exhibition. (2012) 1086-1093.

[10] H. K. D. H. Bhadeshia, S. R. Honeycombe. Steels: microstructure and properties, third ed., Butterworth-Heinemann, Oxford, 2011.

[11] S. T. Ahn, D. S. Kim, W. J. Nam. Microstructural evolution and mechanical properties of low alloy steel tempered by induction heating, Journal of Materials Processing Technology. 160 (2005) 54-58. https://doi.org/10.1016/j.jmatprotec.2004.03.019.

[12] B. A. Lindsley and A. R. Marder. The morphology and coarsening kinetics of spheroidized Fe-C binary alloys, Acta Materialia. 46 (1998) 341-351.

[13] R. P. Foley, R. K. Weiss, S. W. Thompson, G. Krauss. Tempering behaviour of martensite plate steels produced by direct quench and reaustenitize- and -quench processing, in: R. Ashahani, G. Tither (Eds.), International symposium on low-carbon steels for the 90's. 1993.

[14] J. R. Driscoll. An investigation into the microstructure and precipitation characteristics of reheated quenched and tempered 701 steel (RQT701) quenched from 925 °C in austenite to an autotempered martensitic microstructure, and tempered at 580 °C, 600 °C and 620 °C for between 1 and 100 hours. MRes thesis, University of Birmingham, 2014.

[15] G. R. Speich and W. C. Leslie. Tempering of steel, Metallurgy Transactions. 3 (1972) 1043-1054. https://doi.org/10.1007/bf02642436.

[16] G. Miyamoto, J. C. Oh, K. Hono, T. Furuhara, T. Maki. Effect of partitioning of Mn and Si on the growth kinetics of cementite in tempered Fe–0.6 mass% C martensite, Acta Materialia. 55 (2007) 5027-5038. https://doi.org/10.1016/j.actamat.2007.05.023.

[17] C. Zhu, X. Y. Xiong, A. Cerezo, R. Hardwicke, G. Krauss, G. D. W. Smith. Three-dimensional atom probe characterization of alloy element partitioning in cementite during tempering of alloy steel, Ultramicroscopy. 107 (2007) 808-812. https://doi.org/10.1016/j.ultramic.2007.02.033.

[18] L. Chang, G. Smith. The silicon effect in the tempering of martensite in steels, 31st International Field Emission Symposium, Journal de Physique Colloques. 45 (1984) C9-397-401. https://doi.org/10.1051/jphyscol:1984966.

[19] R. N. Caron, G. Krauss. The tempering of Fe-C lath martensite, Metallurgical Transactions. 3 (1972) 2381-2389. https://doi.org/10.1007/bf02647041.

[20] W. J. Nam, C. M. Bae. Coarsening behavior of cementite particles at a subcritical temperature in a medium carbon steel, Scripta Materialia. 41 (1999) 313-318. https://doi.org/10.1016/s1359-6462(99)00168-2.

[21] W. J. Nam. Effect of initial microstructure on the coarsening behavior of cementite particles, ISIJ International. 39 (1999), 1181-1187. https://doi.org/10.2355/isijinternational.39.1181.

[22] S. Yamasaki. Modelling precipitation of carbides in martensite steels. PhD thesis, University of Cambridge, 2004.

[23] K. Tamaki, J. Suzuki. Precipitation of carbides during tempering of Cr-Mo steels, Research report of the faculty of engineering, Mie University. 7 (1982) 39-52.

[24] A. Výrostková, A. Kroupa, J. Janovec, M. Svoboda. Carbide reactions and phase equilibria in low alloy Cr-Mo-V steels tempered at 773-993 K. Part I: Experimental measurements, Acta Materialia. 46 (1998) 31-38. https://doi.org/10.1016/S1359-6454(97)00238-3.

[25] C. Pandey, A. Giri, M. M. Mahapatra. Evolution of phases in P91 steel in various heat treatment conditions and their effect on microstructure stability and mechanical properties, Materials Science and Engineering A. 664 (2016) 58-74. https://doi.org/10.1016/j.msea.2016.03.132.

[26] W. Steven, A. G. Haynes. The temperature formation of martensite and bainite in low-alloy steels, some effects of chemical composition, Journal of Iron and Steel Institute. 183 (1956) 349-359.

[27] M. G. H. Wells. An electron transmission study of the tempering of martensite in an Fe-Ni-C alloy, Acta Metallurgica. 12 (1964) 389-399. https://doi.org/10.1016/0001-6160(64)90009-4,.

[28] W. C. Leslie, G. C. Rauch. Precipitation of carbides in low-carbon Fe-Al-C alloys, Metallurgical Transactions A. 9 (1978) 343-349. https://doi.org/10.1007/bf02646383.

[29] G. E. Totten. Steel heat treatment: metallurgy and technologies, second ed., Taylor & Francis, Oregon, 2006.

[30] G. Y. Lai. On the precipitation of epsilon-carbide in lower bainite, Metallurgical Transactions A. 6A (1975) 1469-1471. https://doi.org/10.1007/bf02641942.

[31] S. W. Thompson. Structural characteristics of transition-iron-carbide precipitates formed during the first stage of tempering in 4340 steel, Materials Characterization. 106 (2015) 452-462. https://doi.org/10.1016/j.matchar.2015.05.030.

[32] H. K. D. H. Bhadeshia, S. A. David, J. M. Vitek, R. W. Reed. Stress induced transformation to bainite in Fe–Cr–Mo–C pressure vessel steel, Materials Science and Technology, 7 (1991) 686-698. https://doi.org/10.1179/026708391790184915.

[33] X-ray Powder Data File (circ. 539 4 3), card for α iron, US National Bureau of Standards, 1955.

[34] Y. Ju, A. Goodall, C. Davis, M. Strangwood. Characterisation of precipitation and coarsening of carbides during tempering in a low alloyed quenched and tempered steel, THERMEC International Conference on Processing & Manufacturing of Advanced Materials Processing, Fabrication, Properties, Applications, Materials Science Forum (In press), 2018.

[35] G. Krauss. Martensitic transformation, structure and properties in hardenable steels, Metallurgical Society of AIME. (1978) 229-248.

[36] P. B. Hírsch and F.J. Humphreys. Plastic deformation of two-phase alloys containing small nondeformable particles, in: A. S. Argon, E. Orowan (Eds), Physics of strength and plasticity, MIT Press, Cambridge, 1969.

[37] R. C. Weast. CRC handbook of chemistry and physics, 56th ed., CRC Press, Florida, 1976.

[38] I. Kaur, W. Gust, L. Kozma. Handbook of grain and interphase boundary diffusion data, Ziegler Press, 1989.

[39] I. Kaur, Y. Mishin, W. Gust. Fundamentals of grain and interphase boundary diffusion, third ed., John Wiley & Sons Inc., New York, 1995.

[40] K. J. Irvine, F. B. Pickering. The tempering characteristics of low carbon low alloy steels, Journal of the Iron and Steel Institute. 194 (1960) 137-153.

[41] E. C. Bain, H. W. Paxton. Alloying elements in steel, second ed., ASM, Metals Park, Ohio, 1961.